Int. J. Appl. Ceram. Technol., 8 [4] 809–814 (2011)
DOI:10.1111/j.1744-7402.2010.02511.x

International Journal of
Applied Ceramic TECHNOLOGY
Ceramic Product Development and Commercialization

Permeability Enhancement in Porous-Sintered Reaction-Bonded Silicon Nitrides

Young-Jo Park* and Hai-Doo Kim

Engineering Ceramics Research Group, Korea Institute of Machinery and Materials, 66 Sangnam-Dong, Changwon-Shi, Gyeongsangnam-Do 641-010, Korea

John W. Halloran

Department of Materials Science and Engineering, University of Michigan, Ann Arbor, Michigan 48109

Pressure drop across filter materials is critical for the effective performance of various kinds of filtering system. To evaluate the feasibility of lowering the pressure drop of porous sintered reaction-bonded silicon nitrides, permeability tests were conducted for specimens with different porosity and pore structure. The results showed that pore former size is a minor factor, while permeability (κ) had a strong dependency on the amount of pore former. Prolonged sintering time (2 h vs 10 h at 1700°C) increased the permeability by increasing the effective pore diameter, which compensates for the observed decrease in total porosity.

Introduction

Since the early 1990s, there has been research into nonconventional structural applications of Si_3N_4 ceramics. In particular, because of its planned usage as device substrates,[1–6] as machinable ceramics,[7,8] and as filtering media,[9–14] many technological investigations have concentrated on the enhancement of thermal conductivity and development of porous bodies with controlled microstructures, for example crystallinity, texture, grain morphology, and pore size distribution. A significant disadvantage of engineering ceramics is the difficulty in machining them after sintering, which leads to high

This study was supported by the CEFV (Center for Environmentally Friendly Vehicles) of the Eco-STAR project from the MOE (Ministry of Environment), Korea.
*yjpark87@kims.re.kr

machining cost and has kept them from widespread usage. By adjusting sintering additive characteristics, both type and amount, porous Si_3N_4 ceramics have been developed using the same sintering process used to obtain dense Si_3N_4 ceramics. In addition to providing machinability, porous ceramics have many industrial applications as filtering materials, including use in high-temperature gas filters, separation membranes, and as catalyst supports. The acicular grain morphology of Si_3N_4 ceramics[15,16] with its optimum combination of filtering efficiency and permeability, makes these materials excellent filtering media. The complex pore channels of the rod-like grains provide large surface areas to trap particulate matters, while the larger number of channels compared with that of equiaxed-grained ceramics provides more paths as clogging begins. Further, Si_3N_4 ceramics have reported to offer high thermal shock resistance and superior mechanical/chemical stability at high temperatures, which are required properties for high temperature and corrosive environment applications. Previous research in the field of porous Si_3N_4 ceramics have concentrated on strength sustainment of the closed pore body[7,13,17–19] and microstructural evolution of whisker-like grains.[10–12]

In this study, metal silicon powder, which is less expensive than Si_3N_4 powder, was selected as a starting material and a reaction-bonding process[20–22] followed by postsintering[23–27] were used to produce an Si_3N_4 filter substrate. However, the diameter of pore channels in the porous sintered reaction-bonded silicon nitrides (SRBSNs) is usually restricted to $\sim 1\,\mu m$ owing to: (1) the nitriding mechanism involving gas phase and solid phase and (2) the limit of grain growth in the porous body by liquid-phase sintering vehicle ($d = 1$–$2\,\mu m$).[3–5] To take advantage of the excellent thermomechanical properties and the peculiar filtration mechanism of Si_3N_4 ceramics, a certain level of permeability is needed in a filter substrate, because pressure drops across the filter diminishes efficiency by increasing back-pressure. The goal of this research was to gain knowledge of the factors enhancing permeability of SRBSNs. Both the amount and size of pore former as well as postsintering time at fixed temperatures, were the parameters investigated in the current research.

Experimental Procedure

The metal silicon powder used for the present study was commercially available (composition by weight: $>98.6\%$ Si, 0.4% Fe, 0.2% Al, 0.2–1.0% O; particle size distribution, $d_{50} = 7\,\mu m$, Sicomill® grade 2, Vesta Ceramics, Ljungaverk, Sweden). Commonly adopted oxide sintering additives, such as Y_2O_3 (99.99%, $d_{50} = 0.7\,\mu m$, Grade C, H. C. Stark, Goslar, Germany) and Al_2O_3 (AKP-30, 99.99%, $d_{50} = 0.31\,\mu m$, Sumitomo, Tokyo, Japan) were used. The total amount of sintering additives was fixed at 2.3% by weight, keeping the weight ratio of $Y_2O_3/Al_2O_3 = 3.54$. Weight percentages of sintering additives were calculated based on the amount of Si_3N_4, assuming perfect nitridation of raw silicon powder into Si_3N_4. polymethyl methacrylate (PMMA, Aldrich, St. Louis, MO) was used as a pore former. Two different sizes and weights, $\varphi = 8\,\mu m$ (20 g) and 50 μm (30 g), were used. In all specimens, 20 g of Si_3N_4 (E-10 grade, 1.24% O by weight, α-fraction $>95\%$, $d_{50} = 0.3\,\mu m$, Ube Industries, Ube, Japan) were added to 80 g of Si. Specimen compositions and nomenclature are summarized in Table I. Approximately 50 g of powder mixture comprising Si powder and other components were thoroughly mixed in a nylon jar with Si_3N_4 balls and ethanol as milling media for 4 h using a planetary milling machine. After the mixture had been dried using a rotating evaporator, it was sieved to a particle size of $<150\,\mu m$. The resulting powder mixtures were uniaxially pressed into cylinder shapes and subsequently cold isostatically pressed at 200 MPa to prepare specimens measuring 23 mm in diameter (φ) and 1.1 mm in height (t). After shaping, the specimens were heated in 95% N_2/5% H_2 atmosphere flowing at 150 cm^3/min in a horizontal tube furnace. The nitriding reaction was con-

Table I. Composition and Nomenclature of Specimens

Specimen	Si (g)	Si_3N_4 (g)	Y_2O_3 (g)	Al_2O_3 (g)	PEG (g)	PMMA (g)	Additive (wt%)
S20	80	20	2.87	0.81	3	20 ($d_{50} = 8\,\mu m$)	2.3
S30	80	20	2.87	0.81	3	30 ($d_{50} = 8\,\mu m$)	2.3
L20	80	20	2.87	0.81	3	20 ($d_{50} = 50\,\mu m$)	2.3

PMMA, polymethyl methacrylate; PEG, polyethylene glycol.

ducted at 1350°C for 3 h. A maximum of five specimens from the various trials were placed upon a boron nitride (BN)-coated graphite plate inside an Al_2O_3 tube. The specimens were placed upright with their edges fitting in a small hole on the graphite plate so that contamination and temperature gradient were minimized through minimum contact between specimen and graphite plate. The current configuration of specimens also maximized the surface area where nitrogen penetration commences. The nitridation rate was calculated from the weight change before and after the nitriding process. In preparation for the postsintering of the as-nitrided specimens (reaction-bonded silicon nitrides [RBSNs]), the samples taken from the nitriding furnace were placed upon a BN-coated graphite crucible filled with Si_3N_4 packing powder. Sintering was carried out in a graphite resistance furnace at 1700°C for either 2 or 10 h under nitrogen gas pressure of 0.1 MPa. Flow rate and permeability of nitrogen gas were measured using disk specimens after thinning to $t \leq 0.8$ mm. The flow rate was recorded as the input pressure was gradually increased using a porometer (CFP-1200-AEL; Porous Materials Inc., Ithaca, NY). The microstructural development of the SRBSN specimens was determined using scanning electron microscopy (SEM) investigation (JSM-6700F; JEOL, Tokyo, Japan) on the fracture surface. Pore size and its distribution were characterized using mercury porosimetry (Autopore IV 9510; Micromeritics, Norcross, GA). The number of samples for the characterization by both SEM and mercury porosimetry was two for each composition.

Results and Discussion

A Si_3N_4 in Si powder mixture serves as a diluent preventing an explosive exothermic reaction in the course of nitriding. In addition to stabilizing the nitriding reaction, addition of Si_3N_4 has been used to fabricate porous structures by maintaining the pore size of the original PMMA after it burns by heating. Authors have reported that the pore structure is determined by the Si to the pore former size ratio.[28] Thus, increased packing density by means of adding small Si_3N_4 particles between larger Si particles should create a stable strut structure after the decomposition of the pore former. In this study, PMMA of $\varphi = 8$ and 50 μm were used to investigate the effect of pore size on permeability. Without the addition of Si_3N_4, the larger pores were expected to collapse with only the smaller pores surviving.

Variations in nitridation rates and porosities for RBSN specimens are plotted in Fig. 1. Assuming both perfect nitridation of Si powder and zero weight loss of compact mixtures during the nitriding process, the nitridation rate (R_N) is

$$R_N(\%) = 100 \frac{W_f - W_i}{W_{Si}} \frac{100}{66.5} \quad (1)$$

where W_f is the weight of nitrided compacts comprising unreacted Si, reaction product Si_3N_4, and sintering additives, W_i is the weight of the prenitrided compact, and W_{Si} is the weight of Si in the prenitrided compact. Perfect nitridation of Si into Si_3N_4 is accompanied by a 66.5% weight gain, which is represented as a constant in the denominator of Eq. (1). This nitridation rate only represents the degree of reaction completon, and is not a quantitative measure of the amount of nitrided Si_3N_4. The highest and lowest nitridation rates were measured for S30 and L20 specimens, respectively. The S30 specimen contained the largest amount of PMMA, which enabled the nitrogen gas to access the compacted mixture more easily. The lowest nitridation rate for the L20 specimen is attributed to the thick strut structure owing to the larger size of the PMMA. Although the same amount of PMMA was blended into the S20 and L20

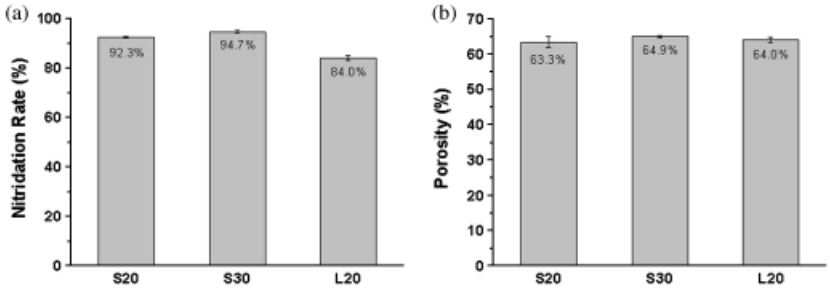

Fig. 1. Measurement of (a) nitridation rate and (b) porosity of reaction-bonded silicon nitrides nitrided at 1350°C for 3 h.

specimens, a slightly higher nitridation rate was achieved in S20. The thicker strut structure in L20 than in S20 is postulated to have hindered the nitriding reaction. The porosity of S30 was marginally greater than those of S20 and L20 in spite of the difference in the amount of PMMA used. As noted in Fig. 1a, the large nitridation rate in S30 resulted in the largest weight gain, and produced nearly similar porosity in all specimens. Shrinkage of the nitrided compacts was less than 0.1%, which is typical for reaction bonding of Si compacts. For nitridation rates >90%, Si peaks are not detected by X-ray diffraction (XRD) and nitridation is considered to be nearly complete.[27]

By postsintering of RBSN at 1700°C, a slight amount of weight loss, 2–3%, occurred by evaporation. Nearly similar porosities of ≈ 60% were measured for all specimens (Fig. 2a). Porosity in 10-h-sintered specimens was slightly lower than in 2 h specimens, which may be the result of increased shrinkage during the prolonged sintering time. Porosity of S20 decreased the most, which was assumed to be a result of the largest amount of shrinkage (Fig. 2b). The smallest shrinkage in L20 is attributed to the relatively inhomogeneous distribution of the liquid phase owing to the existence of the largest pore former.

In Fig. 3, the flow rate, which is related to permeability, is plotted as a function of differential pressure. An increase in sintering time from 2 h (solid symbol) to 10 h (open symbol) markedly increased flow rates. The flow rate of S30 specimens was superior to that of S20 specimens, even though the total porosity values of the two specimens were similar. Flow rates of S20 and L20 were similar for specimens sintered for 2 h, but S20 was more permeable than L20 with an increase of sintering time to 10 h.

To explain the anomalous observation that SRBSNs of lower porosity allowed increased flow, pore channel sizes were measured by mercury porosimetry (Fig. 4). Median pore diameter increased with sintering time for all specimens, which matches the effect of sintering time on the flow rate shown in Fig. 3. Although total porosity level is similar, the larger pore

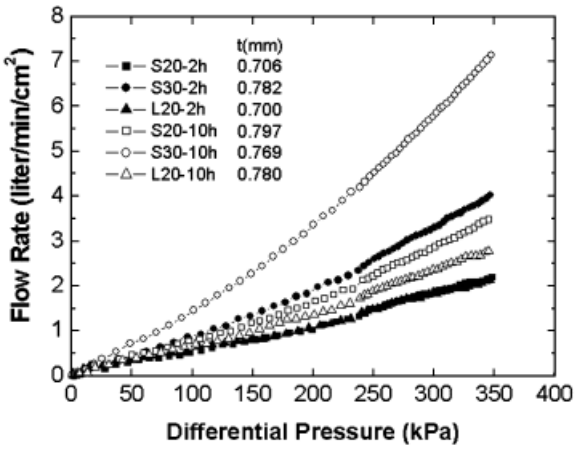

Fig. 3. Measurement of flow rate for sintered reaction-bonded silicon nitrides postsintered at 1700°C for 2 and 10 h.

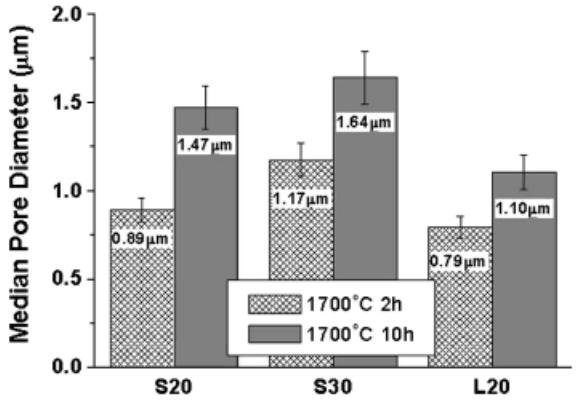

Fig. 4. Measurement of pore channel size for sintered reaction-bonded silicon nitrides postsintered at 1700°C for 2 and 10 h.

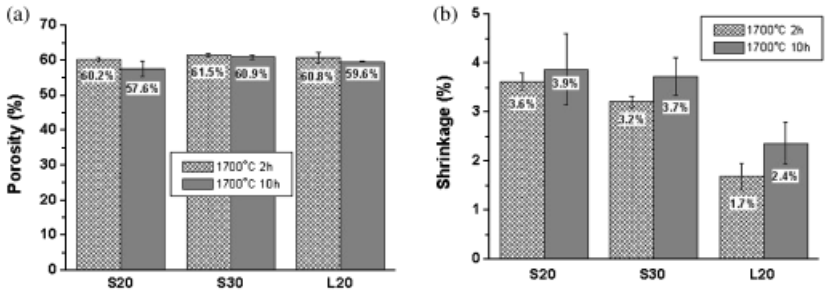

Fig. 2. Measurement of (a) porosity and (b) shrinkage of sintered reaction-bonded silicon nitrides postsintered at 1700°C for 2 and 10 h.

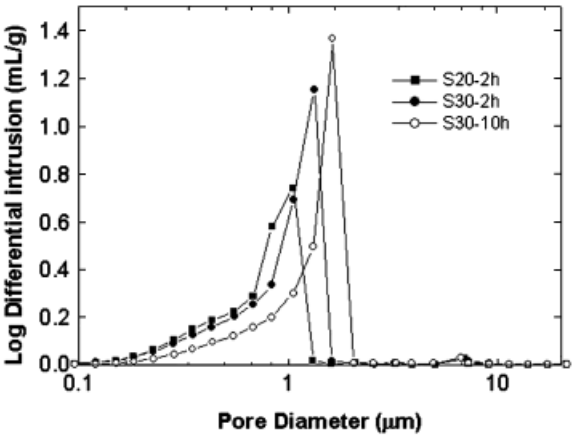

Fig. 5. Measurement of pore channel size and corresponding frequency for sintered reaction-bonded silicon nitrides postsintered at 1700°C for 2 and 10 h.

channel size in S30 than S20 supports the superior flow rate in S30. Sintering time dependency between S20 and L20 may also be explained by pore diameter. Both specimens show similar permeability and pore size after 2 h of sintering, and the higher flow rate of S20 compared with L20 may be attributed to the larger pore size in S20. The results indicate that the use of a smaller pore former is effective for flow rate increases when the same amounts of pore former are blended. It is inferred that narrow pore channels are dominantly formed in the thick strut structure of L20. In addition to the median pore diameter, pore frequency of the selected specimens was plotted to further investigate the enhanced flow rate (Fig. 5). The highest pore frequency was observed in the 10-h-sintered S30 specimens. We conclude that the combination of higher median pore size and higher pore frequency resulted in the increased flow rate.

Figure 6 illustrates the morphology of fracture surfaces of SRBSNs. Observation of pore structures in SEM photographs provided the visual evidence of permeability promotion in the porous SRBSNs. The addition of a smaller pore former is effective, because the larger pore former results in thicker strut structures when the same amount of pore former is used. Increased effective pore diameter by increasing the sintering time is obvious in Fig. 6.

Fluid flow through porous media has been reported to follow Darcy's empirical equation

$$\frac{Q}{A} = \frac{\kappa}{\mu}\frac{\Delta P}{L} \tag{2}$$

where Q is flow, A is surface area, κ is Darcy's permeability, μ is dynamic viscosity, ΔP is pressure drop, and L is length of the medium. In Eq. (2), Permeability (κ) characterizes the flow property of the medium and is directly related to pore diameter through the Kozeny–Carmen equation

$$\kappa = \frac{d^2}{\tau}\frac{\phi^3}{(1-\phi)^2} \tag{3}$$

where d is pore diameter, τ is tortuosity factor, and φ is porosity. Permeability (κ) was measured using the same experimental charges used when the data in Fig. 3 were acquired. Normalized permeability, $k \cdot (1-\varphi)^2/\varphi^3$, as a function of the square of pore diameter, d^2, is plotted in Fig. 7. The linearity of the fitted line supports the find-

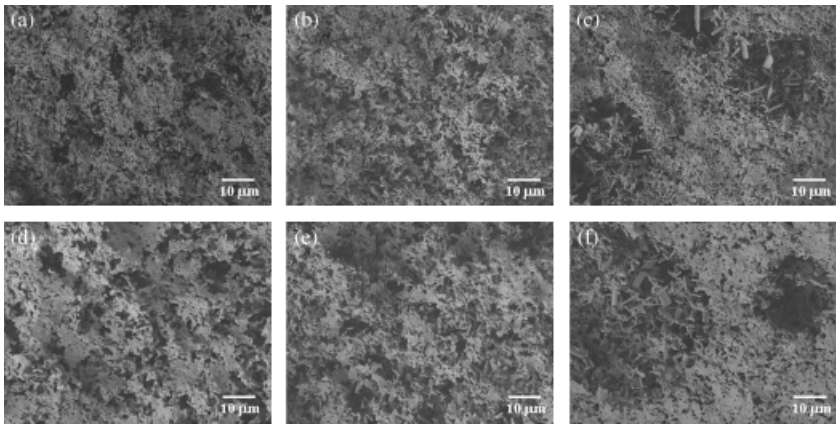

Fig. 6. Fracture surfaces of sintered reaction-bonded silicon nitrides postsintered at 1700°C for 2 h (a–c) and 10 h (d–f). (a and d) S20, (b and e) S30, and (cand f) L20.

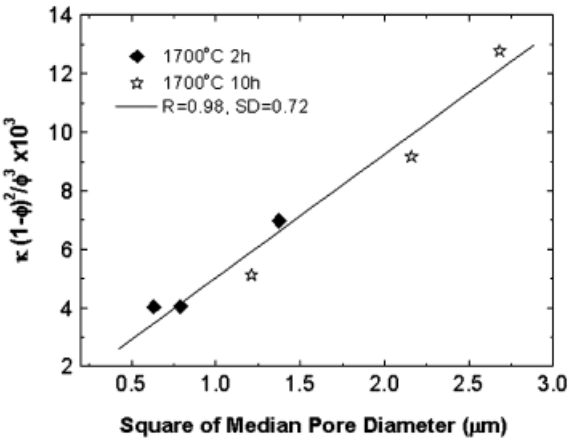

Fig. 7. Relationship between Darcy permeability (k) and the square of pore diameter (d^2) using Kozeny–Carmen equation.

ings in this study and indicates that flow properties are dominated, not by porosity, but by pore diameter.

Conclusions

In order to optimize the performance of SRBSN filtering systems, increasing the permeability of porous SRBSNs was investigated for the specimens containing 20–30 part pore former. The results revealed that pore channel diameter is the dominant factor in controlling the permeability for a given total porosity. Use of smaller pore former material is effective, because such material produces homogeneously thinner strut structures compared with the thicker strut structures produced from larger pore former material. Although a slightly decreased porosity may result from increased shrinkage after a prolonged sintering time, the widened pore channel induced by pore coalescence during prolonged sintering resulted in enhanced permeability.

References

1. M. Kitayama, K. Hirao, M. Toriyama, and S. Kanzaki, "Thermal Conductivity of β-Si_3N_4: I, Effects of Various Microstructural Factors," *J. Am. Ceram. Soc.*, 82 [11] 3105–3112 (1999).
2. M. Kitayama, K. Hirao, A. Tsuga, K. Watari, M. Toriyama, and S. Kanzaki, "Thermal Conductivity of β-Si_3N_4: II, Effect of Lattice Oxygen," *J. Am. Ceram. Soc.*, 83 [8] 1985–1992 (2000).
3. M. Kitayama, K. Hirao, K. Watari, M. Toriyama, and S. Kanzaki, "Thermal Conductivity of β-Si_3N_4: III, Effect of Rare Earth (RE = La, Nd, Gd, Y, Yb and Sc) Oxide Additive," *J. Am. Ceram. Soc.*, 84 [2] 353–358 (2001).
4. K. Watari, K. Hirao, M. E. Brito, M. Toriyama, and S. Kanzaki, "Hot Isostatic Pressing to Increase Thermal Conductivity of Si_3N_4 Ceramics," *J. Mater. Res.*, 14 [4] 1538–1541 (1999).
5. H. Yokota and M. Ibukiyama, "Microstructure Tailoring for High Thermal Conductivity of β-Si_3N_4 Ceramics," *J. Am. Ceram. Soc.*, 86 [1] 197–199 (2003).
6. N. Hirosaki, Y. Okamoto, F. Munakata, and Y. Akimune, "Effect of Seeding on the Thermal Conductivity of Self-Reinforced Silicon Nitride," *J. Eur. Ceram. Soc.*, 19 2183–2187 (1999).
7. C. Kawai and A. Yamakawa, "Effect of Porosity and Microstructure on the Strength of Si_3N_4: Designed Microstructure for High Strength, High Thermal Shock Resistance, and Facile Machining," *J. Am. Ceram. Soc.*, 80 [10] 2705–2708 (1997).
8. J. F. Yang, Z. Y. Deng, and T. Ohji, "Fabrication and Characterization of Porous Silicon Nitride Ceramics Using Yb_2O_3 as Sintering Additive," *J. Eur. Ceram. Soc.*, 23 371–378 (2003).
9. N. Miyakawa, H. Sato, H. Maeno, and H. Takahashi, "Characteristics of Reaction-Bonded Porous Silicon Nitride Honeycomb for DPF Substrate," *JSAE Rev.*, 24 269–276 (2003).
10. C. Kawai and A. Yamakawa, "Network Formation of Si_3N_4 Whiskers for the Preparation of Membrane Filters," *J. Mater. Sci. Lett.*, 17 873–875 (1998).
11. C. Kawai and A. Yamakawa, "Crystal Growth of Silicon Nitride Whiskers through a VLS Mechanism Using SiO_2–Al_2O_3–Y_2O_3 Oxides as Liquid Phase," *Ceram. Int.*, 24 135–138 (1998).
12. C. Kawai, T. Marsuura, and A. Yamakawa, "Separation-Permeation Performance of Porous Si_3N_4 Ceramics Composed of β-Si_3N_4 Grains as Membrane Filters for Microfilteration," *J. Mater. Sci.*, 34 893–896 (1999).
13. J. F. Yang, G. J. Zhang, and T. Ohji, "Fabrication of Low-Shrinkage, Porous Silicon Nitride Ceramics by Addition of a Small Amount of Carbon," *J. Am. Ceram. Soc.*, 84 [7] 1639–1641 (2001).
14. D. Chen, B. Zhang, H. Zhuang, and W. Li, "Combustion Synthesis of Network Silicon Nitride Porous Ceramics," *Ceram. Int.*, 29 363–364 (2003).
15. M. Kramer, M. J. Hoffmann, and G. Petzow, "Grain Growth Kinetics of Si_3N_4 During α/β-Transformation," *Acta Metall. Mater.*, 41 [10] 2939–2947 (1993).
16. A. J. Pyzik and D. R. Beaman, "Microstructure and Properties of Self-Reinforced Silicon Nitride," *J. Am. Ceram. Soc.*, 76 [11] 2737–2744 (1993).
17. C. Kawai, "Effect of Grain Size Distribution on the Strength of Porous Si_3N_4 Ceramics Composed of Elongated β-Si_3N_4 Grains," *J. Mater. Sci.*, 36 5713–5717 (2001).
18. Y. Inagaki, N. Kondo, and T. Ohji, "High Performance Porous Silicon Nitrides," *J. Eur. Ceram. Soc.*, 22 2489–2494 (2002).
19. N. Kondo, Y. Inagaki, Y. Suzuki, and T. Ohji, "Fabrication of Porous Anisotropic Silicon Nitride by Using Partial Sinter-Forging Technique," *Mater. Sci. Eng.*, A335 26–31 (2002).
20. A. J. Moulson, "Reaction-Bonded Silicon Nitride: Its Formation and Properties," *J. Mater. Sci.*, 14 1017–1051 (1979).
21. H. M. Jennings, "On reactions between Silicon and Nitrogen," *J. Mater. Sci.*, 18 951–967 (1983).
22. G. Ziegler, J. Heinrich, and G. Wotting, "Relationships between Processing, Microstructure and Properties of Dense and Reaction-Bonded Silicon Nitride," *J. Mater. Sci.*, 22 3041–3086 (1987).
23. A. Giachello and P. Popper, "Post-Sintering Of Reaction-Bonded Silicon Nitride," *Ceram. Inter.*, 5 [3] 110–114 (1979).
24. J. A. Mangels and G. J. Tennenhouse, "Densification of Reaction-Bonded Silicon Nitride," *Ceram. Bull.*, 59 [12] 1216–1222 (1980).
25. H. J. Kleebe and G. Ziegler, "Influence of Crystalline Second Phases on the Densification Behavior of Reaction-Bonded Silicon Nitride During Post Sintering Under Increased Nitrogen Pressure," *J. Am. Ceram. Soc.*, 72 [12] 2314–2317 (1989).
26. B. T. Lee, J. H. Yoo, and H. D. Kim, "Size Effect of Raw Si Powder on Microstructures and Mechanical Properties of RBSN and GPSed-RBSN Bodies," *Mater. Sci. Eng.*, A333 306–313 (2002).
27. X. Zhu, Y. Zhou, and K. Hirao, "Post-Densification Behavior of Reaction-Bonded Silicon Nitride (RBSN): Effect of Various Characteristics of RBSN," *J. Mater. Sci.*, 39 5785–5797 (2004).
28. Y. J. Park, E. Choi, H. W. Lim, and H. D. Kim, "Design of Porosity Level for Porous Si_3N_4 Ceramics Manufactured by Nitriding and Post-Sintering of Si Powder Compact," *Mater. Sci. Forum*, 534–536 1017–1020 (2007).